ACS Sustainable Chemistry & Engineering

Research Article

pubs.acs.org/journal/ascecg

Atmospheric Hydrodeoxygenation of Guaiacol over Alumina-, Zirconia-, and Silica-Supported Nickel Phosphide Catalysts

Shin-Kuan Wu,[†] Po-Chen Lai,[†] Yu-Chuan Lin,*[,†] Hou-Peng Wan,[‡] Hom-Ti Lee,[‡] and Ying-Hsi Chang[‡]

[†]Department of Chemical Engineering and Materials Science, Yuan Ze University, 135 Yuan-Tung Road, Chungli, Taoyuan 32003, Taiwan

[‡]Green Energy and Environment Research Laboratories, Industrial Technology Research Institute, Chutung, Hsinchu, 31040 Taiwan

Supporting Information

ABSTRACT: This study investigated atmospheric hydrodeoxygenation (HDO) of guaiacol over Ni_2P-supported catalysts. Alumina, zirconia, and silica served as the supports of Ni_2P catalysts. The physicochemical properties of these catalysts were surveyed by N_2 physisorption, X-ray diffraction (XRD), CO chemisorption, H_2 temperature-programmed reduction (H_2-TPR), H_2 temperature-programmed desorption (H_2-TPD), and NH_3 temperature-programmed desorption (NH_3-TPD). The catalytic performance of these catalysts was tested in a continuous fixed-bed system. This paper proposes a plausible network of atmospheric guaiacol HDO, containing demethoxylation (DMO), demethylation (DME), direct deoxygenation (DDO), hydrogenation (HYD), transalkylation, and methylation. Pseudo-first-order kinetics analysis shows that the intrinsic activity declined in the following order: Ni_2P/ZrO_2 > Ni_2P/Al_2O_3 > Ni_2P/SiO_2. Product selectivity at zero guaiacol conversion indicates that Ni_2P/SiO_2 promotes DMO and DDO routes, whereas Ni_2P/ZrO_2 and Ni_2P/Al_2O_3 enhance DME. These differences were attributed to Ni_2P morphologies on these supports: SiO_2 hosted small Ni_2P particles, which were more active in H-transfer than large Ni_2P clusters supported on ZrO_2 and Al_2O_3. Within the first hour of time on-stream testing, Ni_2P/SiO_2 possessed relatively higher activity than Ni_2P/ZrO_2 and Ni_2P/Al_2O_3. Low coke accumulation and excess phosphorus, which may replenish the Ni_2P phase to maintain its fully phosphided state, were likely responsible for the high activity of Ni_2P/SiO_2 at the outset.

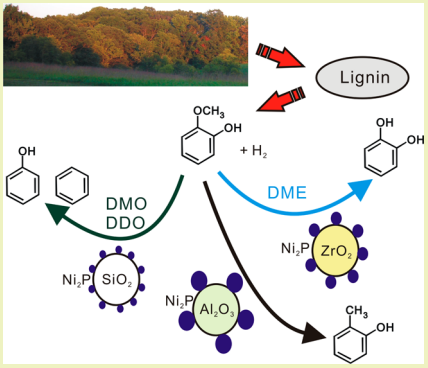

KEYWORDS: *Guaiacol, Hydrodeoxygenation, Nickel phosphide, Supports*

INTRODUCTION

Lignocellulosic biomass-derived fuels and chemicals can help ease society's current reliance on fossil fuels.[1] Selective thermal processing (e.g., gasification[2] and fast pyrolysis[3,4]), liquid phase processing (e.g., liquefaction[5,6] and aqueous phase reforming[7,8]), and hydrodeoxygenation (HDO)[9−11] are potential techniques to transform lignocellulosic biomass into commodity fuels and chemicals. The HDO method is a hydroprocessing technology that removes oxygen in biomass framework through dehydration, releasing water as a byproduct. HDO is an effective method for upgrading various biobased feedstocks such as lignin fractions[12,13] and pyrolysis oils.[14,15]

Compared with other thermochemical processes, HDO is performed at relatively high pressures (ranging between 10 and 100 atm) in H_2-rich environments.[1,10] This limits HDO to biomass upgrading in batch-type scales and thereby increases its capital costs. The pioneer study of Elliott and Baker[16] developed a continuous-feed fixed-bed reactor in an upflow configuration for HDO of bio-oils to gasoline-range cyclic alkanes and aromatics; however, high operating pressures (above 100 atm) are still required.[6,17] This has recently stimulated a boom in continuous gas-phase HDO at low pressures. Oyama et al.[18] reported that the HDO of guaiacol, a lignin model compound, can be conducted under atmospheric pressure in a continuous fixed-bed system through silica-supported transition metal phosphides, including Ni_2P, Fe_2P, MoP, Co_2P, and WP. Among these catalysts, Ni_2P/SiO_2 displayed the highest HDO activity, with benzene and phenol as major products. The Gates group[19] investigated HDO of lignin-derived species (e.g., guaiacol, anisole, and 4-methylanisole) by Pt catalysts. Detailed HDO reaction networks and kinetics of major reaction pathways were reported. Hydrogenolysis, which breaks C−O bonds without oxygen removal from the model species, is the most kinetically significant route in the HDO network. Resasco et al.[20,21] surveyed guaiacol and anisole HDO over Pt catalysts, either as a powder or in monolith form. Bifunctional catalysts (i.e., Pt−Sn or Pt/HBeta) achieve superior activities and stabilities more than monometallic Pt catalysts. This is attributed to the alloy phase of Pt−Sn and metal−acid site interaction of Pt/HBeta.[20] Table 1 presents a summary of earlier studies on the gas-phase HDO of lignin-based compounds.

Table 1 shows that Pt and transition metals supported on silica and alumina are commonly used in the gas-phase HDO.

Received: December 5, 2012
Revised: January 17, 2013
Published: January 25, 2013

   dx.doi.org/10.1021/sc300157d | ACS Sustainable Chem. Eng. 2013, 1, 349−358

Table 1. Earlier Studies in Lignin-Based Compounds HDO at Ambient and Low Pressures

entry	active phase	support	space velocity (h^{-1})	T (K)	P (atm)	feed composition (%)	X (%)[a]	$Y_{aromatics}$[b] (%)	ref
1	Ni_2P, Co_2P, Fe_2P, MoP, and WP	SiO_2	1.4 and 59	573	1	0.024% guaiacol with 80% H_2/N_2 as the carrier gas	12−80	0−48	18
2	Pd and CoMo	Al_2O_3	59	573	1	0.024% guaiacol with 80% H_2/N_2 as the carrier gas	1−70	0	18
3	Pt	γ-Al_2O_3	20−100	573	1.4	3% guaiacol, anisole, 4-methylanisole, or cyclohexanone with 29% H_2 in N_2	0−13	<0.1	19,22,23
4	Pt	MgO	11	573	1.4	3% guaiacol with 29% H_2 in He	<9	<0.1	24
5	Pt	H-Beta and SiO_2	<2.5	673	1	2% anisole with 98% H_2 as the carrier	0−100	5−85	20
6	Pt−Sn	carbon nanotubes coated monolith	<0.3	673	1	0.6% guaiacol or anisole with 16.9% H_2/N_2 as the carrier gas	0−100	0−70	21
7	Fe	SiO_2	0.7−9.1	623−723	1	1% guaiacol with 90% H_2/Ar as the carrier gas	20−60	0.4−38	25
8	Co	Kieselguhr	1.2−2.0	673	1	1% guaiacol with 90% H_2/Ar as the carrier gas	60−100	10−0	25

[a]Conversion of lignin-based material. [b]Carbon yield of aromatic products.

Pt has been used to catalyze demethylation (DME), HDO, and hydrogenation (HYD) sequentially in guaiacol HDO,[20] whereas transition metals such as Fe can serve as a hydrogen reservoir, providing H species for HYD/hydrogenolysis.[25] Note that supports also influence HDO chemistry. The protons of surface hydroxyls of an oxide support may interact with the aromatic ring lying planar on the surface or with guaiacol's methoxy and hydroxyl groups.[26,27] This may lead to different catalytic behaviors for catalysts with the same active phase. For example, cyclopentanone, a cyclic deoxygenated species that has never been reported in guaiacol HDO, can be produced by Pt/MgO but not Pt/γ-Al_2O_3.[24] Thus, the nature of support affects HDO chemistry.

Although researchers have examined various catalysts in guaiacol HDO, studies on the effects of support are scarce. Comparative studies can help reveal the involvement of supports in modifying catalyst morphologies and catalytic performance. This study investigates Ni_2P/Al_2O_3, Ni_2P/ZrO_2, and Ni_2P/SiO_2, showing their catalyst characterizations, catalytic activities, and their correlations with HDO chemistry. Results also reveal their on-stream performances in atmospheric guaiacol HDO.

EXPERIMENTAL SECTION

Materials. $Ni(NO_3)_2{\cdot}6H_2O$ (Alfa Aesar, 99%) and $(NH_4)_2HPO_4$ (J.T. Baker, 99%) were used as precursors of the Ni_2P phase. A Ni/P molar ratio of 0.5 was used. Al_2O_3 (Alfa Aesar), ZrO_2 (Alfa Aesar), and SiO_2 (Alfa Aesar) were used as supports. Ni_2P/ZrO_2 and Ni_2P/SiO_2 were prepared by incipient wetness impregnation of an aqueous nickel phosphate solution on the supports. After impregnation, the powder was dried in air at 120 °C for 1 h and then calcined at 500 °C for 6 h. Ni_2P/Al_2O_3 was synthesized by dropwise adding nickel solution to calcined Al_2O_3 until incipient wetness, followed by drying at 120 °C for 1 h and calcining at 500 °C for 6 h. The remaining powder was subsequently impregnated with $(NH_4)_2HPO_4$ solution and subjected to the same thermal treatment as the other catalysts.

The remaining powder was ground and sieved to particles in the range of 40−80 meshes (0.42−0.18 mm). The particles were then reduced in a 80% H_2/N_2 stream (150 mL/min) with a 2 °C/min heating rate from room temperature to 700 °C for 2 h. Because Al_2O_3 interacts strongly with phosphorus,[28,29] Ni_2P/Al_2O_3 was reduced at 900 °C for 2 h. This reduction step transformed phosphate into phosphide.[30] After cooling to ambient temperature in a He stream (100 mL/min), the sample was passivated in a 2% O_2/He stream for 4 h. Approximately 1.6 mmol of Ni was used per gram of support, corresponding to an Ni_2P loading of 11.2 wt %.

Catalyst Characterization. X-ray diffraction (XRD) patterns were acquired on a Shimadzu LabX XRD-6000 with Cu Kα_1 radiation (0.15418 nm). Scans were taken at a scanning rate of 4°/min in a 5−80° angle range (2θ). The voltage and current were set at 40 kV and 30 mA, respectively.

BET surface area measurement, H_2 temperature-programmed reduction (H_2-TPR), H_2 temperature-programmed desorption (H_2-TPD), and CO chemisorption were performed on a Micromeritics Autochem 2920 equipped with a thermal conductivity detector (TCD). Each trial consumed approximately 0.2 g of the passivated sample. Prior to the test, each sample was dehydrated at 150 °C under a N_2 stream (30 mL/min) for 30 min and cooled to room temperature. In BET measurement, a 30% N_2/He stream was used for N_2 physisorption at −196 °C. The specific surface area was estimated by the desorbed N_2 area using the single-point BET equation. In H_2-TPR analysis, phosphate precursors were reduced in a 10% H_2/Ar (30 mL/min) stream at a linearly increasing rate of 5 °C/min to 900 °C. For H_2-TPD, the sample was prereduced in 10% H_2/Ar (30 mL/min) using the same program as H_2-TPR to 700 °C (Ni_2P/SiO_2 and Ni_2P/ZrO_2) or 900 °C (Ni_2P/Al_2O_3) for 2 h. After cooling in a He stream (20 mL/min), H_2-TPD was performed in an Ar stream (30 mL/min) with a 5 °C/min heating rate. The sample pretreatment for CO chemisorption was the same as that for H_2-TPD, and CO chemisorption was conducted at −20 °C using a cryocooler. Pulses of 10% CO/He (2.4 μmol/s) were repeatedly dosed into the system until the sample was completely saturated with chemisorbed CO, and CO uptake was estimated based on the difference of the sum of the CO pulse peak areas between a tested sample and a calibrated volume.

Ammonia pulse chemisorption and temperature-programmed desorption (NH_3-TPD) were performed using a built in-house system. The TCD was equipped to quantify chemisorbed ammonia and record the desorption profile. Each trial consumed approximately 50 mg of the sample. Pulse chemisorption was conducted by injecting 1% NH_3/He (10 mL) pulses, 8 min apart, onto the catalyst bed at 130 °C until achieving a breakthrough. NH_3-TPD was conducted after pulse chemisorption in a He stream from 130 to 600 °C at a heating rate of 10 °C/min. The NH_3 readsorption was negligible at a carrier gas contact time of 5×10^{-4} g/min/mL.[31]

Reactivity Studies. Catalytic tests were performed in a continuous fixed-bed design.[31] This system consisted of a quartz reactor (i.d. = 1.7 cm), two mass flow controllers, and an ice bath cooling trap. The guaiacol (Alfa Aesar, 98%) feeding rate was controlled by a syringe pump (NE-300) and gasified at 210 °C using a 80% H_2/N_2 stream as the carrier (150 mL/min). A guaiacol-containing stream was fed into the system after achieving a stable feeding rate (usually after more than 6 h bypassing). The amount of injected guaiacol was set to be equal to the number of active sites estimated by CO chemisorption. Approximately 0.1 g of the sample was used per trial in activity

Table 2. Characterization Results for Ni_2P Catalysts

catalyst	S_{BET} catalyst/support (m^2/g)	d_{XRD} (nm)	n_{site}[a] (μmol/g)	dispersion[b] (%)	CO uptake (μmol/g)	NH_3 uptake catalyst/support (μmol/g)
Ni_2P/Al_2O_3	90/194	14	87	5	35	211/129
Ni_2P/ZrO_2	47/59	8	153	10	30	205/115
Ni_2P/SiO_2	127/268	6	204	13	26	200/99

[a]Estimated from d_{XRD} based on $n_{site} = S_{eff} \times n \times f$.[30] S_{eff} is the effective surface area of Ni_2P ($S_{eff} = 6/(\rho \times d_{XRD})$: ρ is the density of Ni_2P, 7.09 g/cm^3); n is the mean surface metal atom density, 1.01×10^{15} atoms/cm^2; f is the weight fraction of Ni_2P. [b]Estimated by n_{site}/(1.6 mmol/g of Ni) × 100%.

evaluation. Reaction temperature was set at 300 °C with different weight hourly space velocity (WHSV) values. To investigate the intrinsic chemistry of each catalyst in HDO, kinetic analysis at low guaiacol conversions (<20%) was performed. Detailed experimental conditions of activity evaluation and kinetic analysis were described (see Tables S1 and S2 of the Supporting Information). After testing, the system was flushed with a N_2 stream (120 mL/min) for 3 min to collect residual products and unconverted guaiacol. The cooling trap captured liquid products, including catechol ($C_6H_6O_2$), anisole (C_7H_8O), cresol (C_7H_8O), phenol (C_6H_6O), benzene (C_6H_6), cyclohexanone ($C_6H_{10}O$), and cyclohexanol ($C_6H_{12}O$). Gaseous products, including CH_4, CO, and uncondensed benzene, were collected using a gas bag. Qualitative and quantitative analyses of liquid and gas products were performed using a GC/MS (HP 5890 II GC with 5972 MSD, DB-5MS capillary column, 60 m × 0.25 mm) and a GC TCD/FID equipped with a methanizer (SRI 8610, molecular sieve 13X and silica gel columns). Coke was determined by measuring the weight loss of spent catalyst using a thermogravimetric analyzer (TGA, TA Instruments Q50). The post-reaction sample was first dehydrated in a N_2 stream (60 mL/min) at 130 °C for 1 h. A dehydrated sample was subjected to a thermal program at a 5 °C/min heating rate in air (60 mL/min) from 130 to 600 °C. The weight loss was assumed to be the amount of burnt-off carbon.

Guaiacol conversion (X_{GUA}), carbon yield of product (Y_i), and selectivity (S_i) were defined as follows:

$$X_{GUA} = \frac{(\text{moles of guaiacol})_{in} - (\text{moles of guaiacol})_{out}}{(\text{moles of guaiacol})_{in}} \times 100\% \quad (1)$$

$$Y_i = \frac{\text{moles of carbon in product i}}{\text{moles of carbon in guaiacol}} \times 100\% \quad (2)$$

$$S_i = \frac{\text{moles of carbon in product i}}{\text{the sum of carbon moles in products}} \times 100\% \quad (3)$$

RESULTS AND DISCUSSION

Catalyst Characterization. Table 2 lists the physicochemical properties of tested catalysts, including the surface areas of pure supports, for comparison. All supports suffered considerable surface area losses after anchoring nickel phosphides. The surface area losses may be attributed to fouling and pore blockage by excess phosphorus.[32] Crystallite size estimated by XRD follows the trend of Ni_2P/Al_2O_3 (14 nm) > Ni_2P/ZrO_2 (8 nm) > Ni_2P/SiO_2 (6 nm). The Ni_2P surface concentration and dispersion can be calculated based on the crystallite size, as shown in the fourth and fifth columns of Table 2. Both surface concentration and dispersion increased as Ni_2P/Al_2O_3 < Ni_2P/ZrO_2 < Ni_2P/SiO_2. However, the irreversible CO uptakes were similar, ranging from 26 to 35 μmol/g. The CO chemisorption capacities can be used to estimate surface nickel sites at a 1-to-1 stoichiometry.[18,33] The differences between theoretically calculated Ni sites (n_{site}) and CO uptake is primarily due to the difference of Ni particle size: larger Ni particles chemisorbed less CO than smaller Ni clusters.[33] Another explanation is that Ni sites were blocked by phosphorus, thereby hindering CO chemisorption on nickel phosphides.[34−36]

Figure 1 shows diffractograms of passivated Ni_2P catalysts and the patterns of their corresponding supports. All catalysts

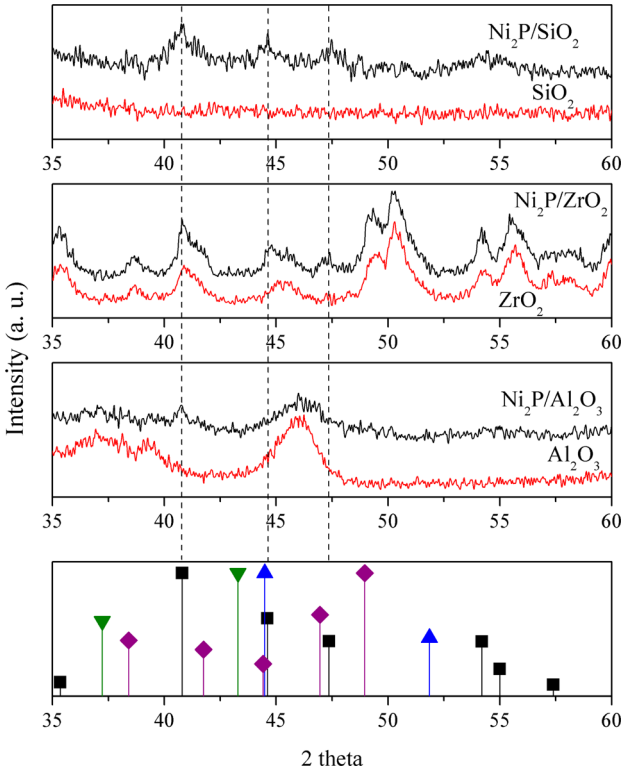

Figure 1. XRD patterns of Ni_2P-supported catalysts and their corresponding supports. The diffraction peaks of Ni_2P (PDF no. 74-1385), $Ni_{12}P_5$ (PDF no. 74-1381), NiO (PDF no. 89-7390), and Ni (PDF no. 87-0712) are designated by ■, ♦, ▼, and ▲ symbols, respectively.

possessed the most intense (1 1 1) reflection (40.7°) of Ni_2P (PDF no. 74-1385). The (2 0 1) and (2 1 0) reflections at 44.6° and 47.4°, respectively, were identified for Ni_2P/ZrO_2 and Ni_2P/SiO_2. These peaks of Ni_2P/Al_2O_3 may be overshadowed by the broad reflection of Al_2O_3 support. Because Al_2O_3 interacts strongly with phosphorus (forming amorphous $AlPO_4$),[28,29] it inhibits Ni_2P synthesis and yields various Ni phases, such as $Ni_{12}P_5$,[35] $NiAl_2O_4$,[37] and NiO.[38,39] However, the strongest reflections of $Ni_{12}P_5$ (PDF no. 74-1381) at 48.9°, $NiAl_2O_4$ (PDF no. 10-0339) at 37.0°, and NiO (PDF no. 89-7390) at 43.3° were absent from Ni_2P/Al_2O_3. A possible explanation is that negligible amounts of different Ni phases were formed or the clusters were too small (less than 5 nm) to be detected by XRD.

Figure 2 shows the TPR profiles of the calcined phosphate precursors of Ni_2P/Al_2O_3, Ni_2P/ZrO_2, and Ni_2P/SiO_2,

dx.doi.org/10.1021/sc300157d | ACS Sustainable Chem. Eng. 2013, 1, 349−358

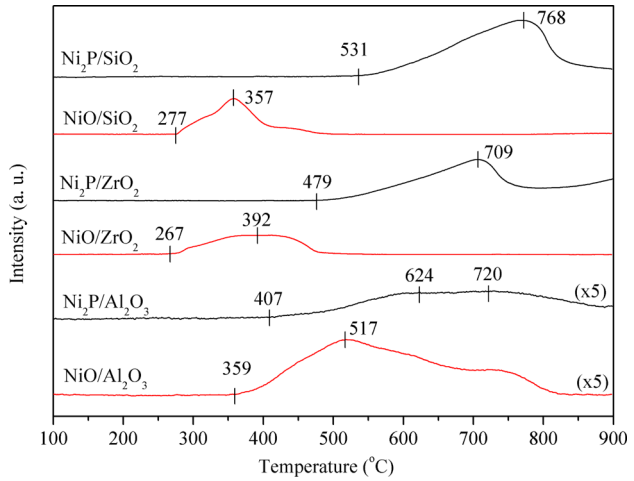

Figure 2. TPR of Ni_2P-supported catalysts; NiO-supported counterparts were also included (red curves).

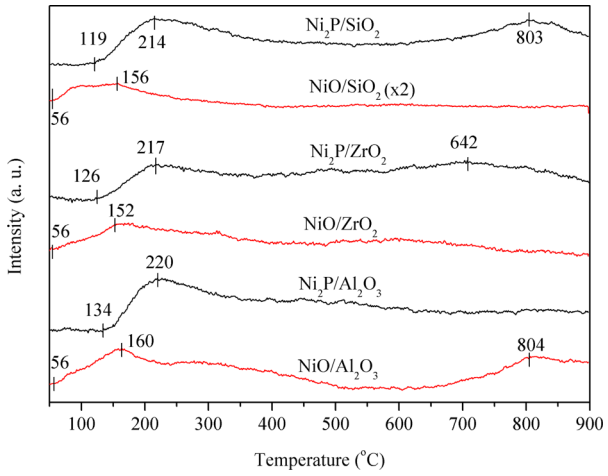

Figure 3. H_2-TPD of Ni_2P-supported catalysts.

including the patterns of NiO/Al_2O_3, NiO/ZrO_2, and NiO/SiO_2 for references. A distinct peak appeared at 768 °C for Ni_2P/SiO_2, and Ni_2P/ZrO_2 displayed a major peak at 709 °C combined with high-temperature reductions above 800 °C. Ni_2P/Al_2O_3 exhibited a comparatively weak H_2 consumption response, which was exaggerated by a multiple of 5. The profile displayed a broad reduction in the range of 400−800 °C with the peaks at 624 °C. The onset reduction temperature decreased in the order of Ni_2P/SiO_2 (531 °C) > Ni_2P/ZrO_2 (479 °C) > Ni_2P/Al_2O_3 (407 °C). The response above 800 °C is related to the reduction of phosphates (e.g., unreduced $(HPO_3H)^-$ or PO_3^-/PO_4^{-3} anions)[40] to PH_3.[32,33]

NiO supported on ZrO_2 and SiO_2 displayed low-reduction temperatures, initiating at approximately 270 °C with major peaks at 350−400 °C. This indicates an interaction between Ni and P in the oxidative precursors, thereby retarding the reduction temperatures of Ni_2P/ZrO_2 and Ni_2P/SiO_2. The onset and maxima reduction temperatures for NiO/Al_2O_3 were similar to that of Ni_2P/Al_2O_3 (about 100 °C in difference), suggesting a weak Ni−P interaction on Ni_2P/Al_2O_3. The broad TPR response also implies the coexistence of different Ni phases. Oyama and Lee[41] conducted the TPR of Ni_2P supported on SiO_2 with low and high surface areas and reported greater reduction temperature by increasing Ni_2P dispersion on high surface area SiO_2. They proposed that small Ni_2P clusters had a strong Ni−P interaction.[41] This is in accordance with this study: the estimated Ni_2P crystallite sizes decreased (Ni_2P/Al_2O_3 (14 nm) > Ni_2P/ZrO_2 (8 nm) > Ni_2P/SiO_2 (6 nm)) following the trend of increasing temperatures of TPR peaks (Ni_2P/Al_2O_3 (624 °C) < Ni_2P/ZrO_2 (709 °C) < Ni_2P/SiO_2 (768 °C)). That is, using SiO_2 as the support yielded the strongest interaction between Ni and P for supported Ni_2P. Conversely, Ni_2P on Al_2O_3 had the weakest Ni−P interaction.

Figure 3 shows the H_2-TPD patterns of Ni_2P-supported catalysts and their NiO-supported counterparts. The desorption of Ni_2P/SiO_2 initiated at 119 °C, showing two distinct peaks at 214 and 803 °C. Ni_2P/ZrO_2 exhibited a broad distribution pattern, with an onset of H_2 desorption at 126 °C, a major hump at 217 °C, and a shoulder at 642 °C. Unlike Ni_2P/SiO_2 and Ni_2P/ZrO_2, Ni_2P/Al_2O_3 showed a strong response at 220 °C, with nearly no desorption detected at 600 °C and higher. NiO-supported catalysts exhibited similar patterns: desorption occurs at 56 °C with a main response at approximately 150−160 °C. The desorption signal at 804 °C and higher for NiO/Al_2O_3 may be the result of surface hydroxyl dehydration. Table 3 presents a summary of the amounts of desorbed H_2, as estimated by H_2-TPD signals. The Ni_2P-supported catalysts generally had greater amounts of overall desorbed H_2 than their respective NiO-supported catalysts, suggesting that the phosphorus in the Ni_2P catalysts plays a role in hydrogen storage.

Table 3. H_2 Desorbed from Ni_2P- and NiO-Supported Catalysts

	amount of desorbed H_2 (μmol/g catalyst)		
catalyst	below 400 °C	above 400 °C	overall
Ni_2P/Al_2O_3	39.6	19.6	59.2
Ni_2P/ZrO_2	27.2	37.2	64.4
Ni_2P/SiO_2	39.7	35.2	74.9
NiO/Al_2O_3	34.4	5.9[a]	40.3[a]
NiO/ZrO_2	31.6	11.0	42.6
NiO/SiO_2	22.7	5.0	27.7

[a]Desorption above 600 °C was excluded because of the possibility of dehydration from the hydroxyls of Al_2O_3.

The H_2-TPD patterns in this study can be categorized into two regions using 400 °C as the demarcation interval.[42,43] The low-temperature desorption is attributed to chemisorbed hydrogen on Ni, and the high-temperature desorption is attributed to H_2 spillover from oxide support to the metal (reverse spillover).[44−46] Chen et al.[47] proposed that the reverse H_2 spillover originated from the PO−H group on the phosphide catalysts. The quantitative analysis in Table 3 reveals that the amounts of desorbed H_2 above 400 °C for Ni_2P catalysts were much higher than those of NiO catalysts. This is in agreement with the previous hypothesis, indicating the reverse H_2 spillover from PO−H species. A close investigation shows that Ni_2P/SiO_2 and Ni_2P/ZrO_2 held approximately the same amounts of reverse H_2 spillover (35.2 and 37.2 μmol/g catalyst, respectively), whereas Ni_2P/Al_2O_3 possessed approximately half (19.6 μmol/g catalyst) of these values. In other words, less phosphorus was available on Ni_2P/Al_2O_3 than on Ni_2P/SiO_2 and Ni_2P/ZrO_2.

Figure 4 illustrates the NH_3-TPD patterns of tested catalysts; plain supports were also presented. Table 2 presents the

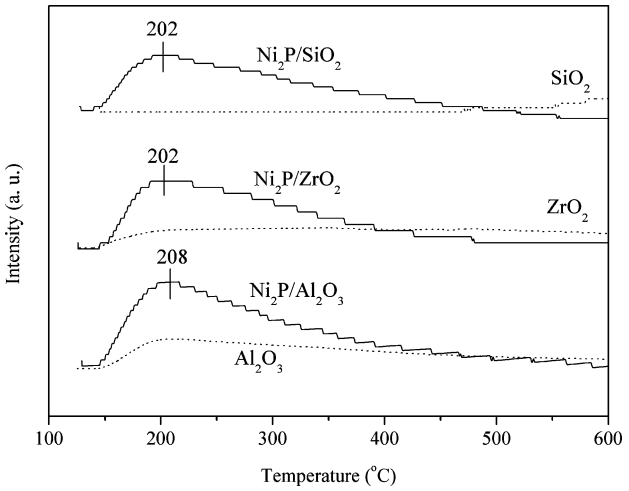

Figure 4. NH_3-TPD of Ni_2P-based catalysts (solid lines) and their corresponding supports (dotted lines).

amounts of chemisorbed NH_3. Desorbed NH_3 declined in the following order of Al_2O_3 > ZrO_2 > SiO_2, in accord with their acidic strengths.[48] The high amount of chemisorbed NH_3 on Al_2O_3 can be attributed to the Lewis acid sites caused by Al^{3+} sites.[49] Desorbed NH_3 increased after anchoring Ni_2P phases. Both Brønsted and Lewis acids can coexist on Ni_2P catalysts. The former is ascribed to PO−H groups, and the latter is ascribed to Ni species in Ni_2P phase.[30] The Lewis acidic Ni is an effective site for molecular activation in hydrotreating processes (e.g., hydrodesulfurization (HDS) of 4,6-dimethyldibenzothiophene and hydrogenation of tetralin).[50] This is because Ni species in Ni_2P have partial positive charges, which facilitate electron transfer for hydrogenation as observed by metallic metals such as Pt and Pd.[47,50] However, the NH_3 desorbed from these two acids was merged and cannot be differentiated. The temperature at peak maximum for each catalyst was nearly identical at approximately 200 °C. The amounts of desorbed NH_3 were relatively close and declined in the following order: Ni_2P/Al_2O_3 (211.2 μmol/g) > Ni_2P/ZrO_2 (205.4 μmol/g) > Ni_2P/SiO_2 (200.4 μmol/g). This indicates that supported Ni_2P phases have similar acidic strengths and acid site numbers, even on different supports.

Reactivity. Table 4 shows the catalytic tests of Ni_2P catalysts in guaiacol HDO at 300 °C. Conversions increased with decreasing WHSV for all catalysts. Ni_2P/SiO_2 displayed the lowest conversions at the same WHSVs, except at WHSV = 0.67 h^{-1}, and all catalysts had their X_{GUA} values greater than 95%. Catechol was the major product at the highest WHSVs (X_{GUA} < 5%). At X_{GUA} less than 5%, trace phenol (2.8%) was detected for Ni_2P/ZrO_2, whereas Ni_2P/Al_2O_3 and Ni_2P/SiO_2 achieved nearly 11% and 20% yields of phenol, respectively, with small amounts of anisole and cresol. A little benzene (2.5%) was identified by Ni_2P/SiO_2 at X_{GUA} = 1%. Phenol was the primary product at X_{GUA} values of 11.7− 29.7%, with the following trend: Ni_2P/ZrO_2 (58.5%) > Ni_2P/SiO_2 (48.9%) > Ni_2P/Al_2O_3 (21.8%). In the same X_{GUA} region, significant benzene (>20%) was observed for Ni_2P/SiO_2, whereas Ni_2P/Al_2O_3 and Ni_2P/ZrO_2 produced less than 5% benzene. More than 30% of catechol was produced by Ni_2P/Al_2O_3. Comparatively, high cresol was generated by Ni_2P/ZrO_2 at X_{GUA} = 29.7%. Benzene and phenol were the main products at X_{GUA} greater than 71.5%. The highest benzene selectivity was achieved when X_{GUA} was close to 100%. At the highest X_{GUA} values, Ni_2P/SiO_2 had the highest benzene selectivity (71.9%), whereas Ni_2P/ZrO_2 (32.4%) and Ni_2P/Al_2O_3 (30.9%) had similar values. Phenol declined in following the order of Ni_2P/ZrO_2 (25.5%) > Ni_2P/Al_2O_3 (13.7%) > Ni_2P/SiO_2 (1.9%) at the highest X_{GUA} points.

Negligible cyclohexanol and cyclohexanone were generated, and cyclohexane was not detected by Ni_2P catalysts. CH_4 and CO were produced within almost all WHSVs, excluding WHSV = 0.67 h^{-1} for Ni_2P/ZrO_2. At X_{GUA} of less than 5%, CH_4 declined in the following order: Ni_2P/ZrO_2 (10.3%) > Ni_2P/Al_2O_3 (7.4%) > Ni_2P/SiO_2 (7.1%). Coke increased as the WHSV decreased. Under the same WHSV, the amount of coke decreased as Ni_2P/Al_2O_3 > Ni_2P/ZrO_2 > Ni_2P/SiO_2.

On the basis of the outcomes of activity evaluation, Figure 5 shows a plausible network for atmospheric guaiacol HDO over Ni_2P catalysts. Four reaction routes are possible: direct deoxygenation (DDO), HYD, DME, and demethoxylation (DMO).[51] DDO involves the direct cleavage of the aromatic carbon−heteroatom bond; therefore, benzene and anisole can be categorized as DDO products. HYD indicates the hydrogenation of the aromatic ring, producing saturated species such as cyclohexanol and cyclohexanone. Trace amounts of these

Table 4. Guaiacol Conversion (X_{GUA}) and Carbon Yield of Product (Y_i) as a Function of WHSV for Atmospheric Guaiacol HDO over Ni_2P-Supported Catalysts

	Ni_2P/Al_2O_3				Ni_2P/ZrO_2				Ni_2P/SiO_2			
WHSV (h^{-1})	0.67	1.33	2.67	5.34	0.67	1.33	2.67	5.34	0.67	1.33	2.67	5.34
X_{GUA} (%)	99.6	97.9	11.7	3.2	96.5	71.5	29.7	3.5	99.5	23.1	1.0	–
Y_i (%)												
phenol	13.7	19.6	21.8	10.8	25.5	35.3	58.5	2.8	1.9	48.9	19.9	–
benzene	30.9	27.2	2.3	0	32.4	28.5	3.7	0	71.9	20.4	2.5	–
anisole	0	0	0.1	0.1	0	0	0.2	0	0	0.2	0.8	–
catechol	0	0	30.6	45.2	0.3	0.2	7.6	67.7	0	0.6	46.7	–
cresol	1.5	2	2.1	2.6	1.3	0.6	6.8	0	0.1	0.8	2.4	–
cyclohexanol	0	0	0	0	0	0	0	0	0	0.1	0	–
cyclohexanone	0	0	0.1	0.2	0	0	0.3	0	0	0.4	0	–
CH_4	1.7	1.9	3.4	7.4	0	0.3	0.3	10.3	2.1	1.1	7.1	–
CO	4.1	4.9	0	0	0	0.8	0.6	0.9	3.6	2.3	0.4	–
coke	40.3	32.7	28.2	24.2	23.6	18.4	17.7	12.9	12.1	11.2	7.2	–
unidentified	7.8	11.7	11.4	9.5	16.9	15.9	4.3	5.4	8.4	14.0	12.9	–

dx.doi.org/10.1021/sc300157d | ACS Sustainable Chem. Eng. 2013, 1, 349−358

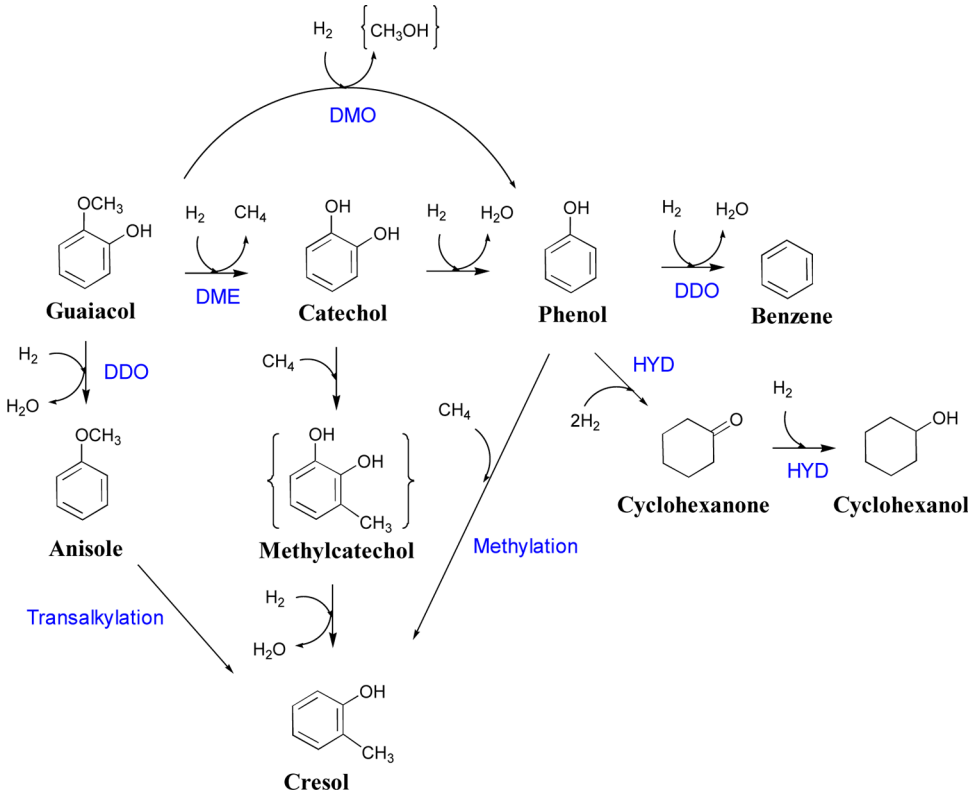

Figure 5. Proposed guaiacol HDO network.

two were generated, suggesting Ni_2P catalysts were inactive for HYD. DME is defined as the removal of a methyl group of guaiacol, yielding catechol and methane as products. DMO involves the extraction of methanol from guaiacol to form phenol. Catechol, CH_4, and phenol were the primary products at the shortest contact time, suggesting that DME and DMO were the initial steps of GUA conversion. The ratio for catechol and CH_4 yields at the lowest X_{GUA} were close to 6:1 for each catalyst, underlining the cleavage of methoxy bond by DME. Unfortunately, methanol could not be separated by the columns of the GCs in this study, but it should be produced accompanied by phenol by the DMO route. Cresol was likely derived from the methyl transfer of anisole (transalkylation),[23,47] dehydration of methylcatechol,[23,51] and methylation of phenol.[22,51] However, these routes are insignificant because methylcatechol is undetectable, and the yield of cresol did not grow with the consumption of anisole and phenol. Intermediates of these routes could be precursors of solid residues (coke).[52] Among these four routes, DDO and DMO are the only oxygen-atom removal pathways.

Guaiacol HDO networks have been proposed by various groups using catalysts such as sulfided CoMo[51,53] and NiMo,[54] Mo nitride,[55,56] and transition metal phosphides[18] in a batch or continuous-flow system under a wide range of H_2 pressures. Although different pathways were suggested, all of them agreed that (i) DMO and DME are the initial steps of guaiacol HDO, yielding methanol and methane as byproducts, (ii) benzene is derived from phenol DDO, (iii) aromatic ring saturation is mostly through phenol HYD instead of benzene hydrogenation, and (iv) methylation and transalkylation produce heavy compounds (e.g., methylcatechol), which are precursors of coke. Note that the route of guaiacol DDO to anisole is identified by limited studies,[20,22,24] including this work. A common point in these studies is that HDO experiments were conducted at a low (1.4 atm) or atmospheric pressure environment. Presumably, operating condition is a key to mediate HDO network.

Figure 6 shows the semi-logarithmic plot of pseudo-first-order kinetics of these catalysts at low guaiacol conversions (less than 20%).[19,22] The well-fitted linear trend indicates that guaiacol HDO obeys first-order kinetics. The rate constants for Ni_2P/Al_2O_3, Ni_2P/ZrO_2, and Ni_2P/SiO_2 are 1.3, 1.5, and 1.2 L (g catalyst)$^{-1}$ h^{-1}, respectively. Accordingly, Ni_2P/ZrO_2 is the most reactive, whereas Ni_2P/SiO_2 is the least reactive in

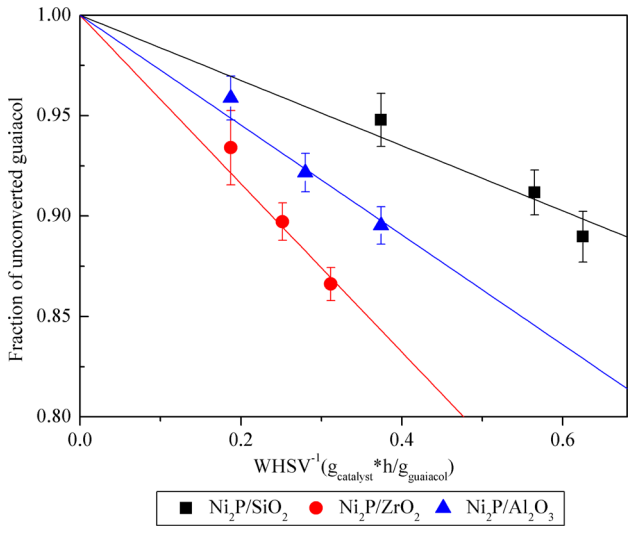

Figure 6. Pseudo-first-order kinetics of guaiacol conversion as a function of inverse WHSV.

dx.doi.org/10.1021/sc300157d | ACS Sustainable Chem. Eng. 2013, 1, 349−358

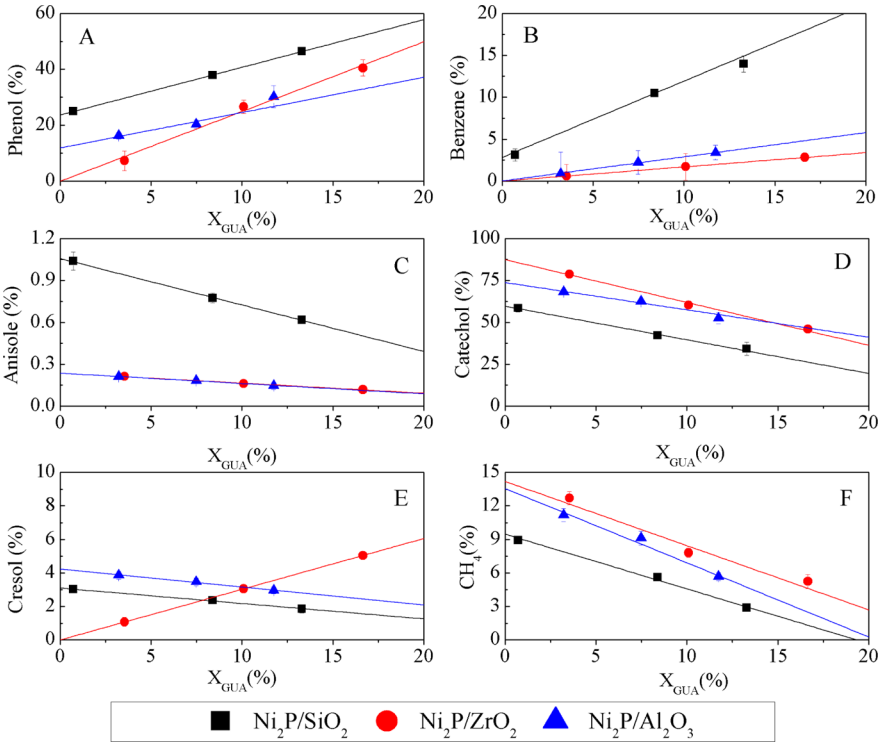

Figure 7. Selectivity of (A) phenol, (B), benzene, (C) anisole, (D) catechol, (E) cresol, and (F) methane as a function of guaiacol conversion under atmospheric HDO conditions at 300 °C. Data for each product were fitted with a linear line and extrapolated to zero conversion.

guaiacol HDO. Gates et al.[22] deployed the same approach to obtain the overall rate constant of guaiacol HDO using Pt/Al_2O_3. Compared to Ni_2P catalysts in this study, an order of magnitude higher rate constant (16.2 L (g catalyst)$^{-1}$ h^{-1}) was achieved, indicating Pt is more active than Ni_2P in guaiacol HDO. However, the noble metal catalyst tends to saturate the benzene ring,[54] which may demand additional H_2 in HDO processing and can downgrade the product's value.

Figure 7 exhibits the selectivity of phenol, benzene, anisole, catechol, cresol, or methane as a function of guaiacol conversion by first-order kinetics. This figure excludes cyclohexanol and cyclohexanone because both of them were negligible (less than 0.4%) in the tested conversion range. Each data set was fitted with a linear trend and extrapolated to zero conversion. The intercept indicates initial product selectivity and has been widely employed in the reaction network analysis of guaiacol HDO.[19,22,23] The selectivity conversion data showed that catechol, methane, and phenol were major products, while benzene, anisole, and cresol (<5%) were minor products. Ni_2P on different supports displayed different trends at zero conversion. Ni_2P/SiO_2 yielded the greatest amount of phenol (23.9%), benzene (2.8%), and anisole (1.1%), which are DMO and DDO products at zero conversion. Ni_2P/ZrO_2 generated the greatest amount of catechol (87.2%) and methane (14.1%), which are both DME species. Ni_2P/Al_2O_3 yielded the most cresol (4.2%).

Because the acidic strengths of these Ni_2P catalysts are similar (as shown in the NH_3-TPD results), the differences in catalytic performance should be attributed to the structural properties of the active phases. According to the EXAFS analysis of Oyama and Lee,[41] two types of Ni sites exist in Ni_2P phases: quasi tetrahedral Ni(1), surrounded by four nearest-neighbor P atoms, and square pyramidal Ni(2), surrounded by five nearest-neighbor P atoms. Both Ni(1) and Ni(2) sites could coexist in a Ni_2P cluster but have different compositions. Small Ni_2P crystallites have strong interactions between Ni and P, yielding more highly P-coordinated Ni(2) sites than Ni(1) sites, large Ni_2P crystallites, and vice versa.[41] Ni(2) has superior HYD ability in HDS of 4,6-dimethyldibenzothiophene[41] because of its capability in hydrogen dissociation and transfer.[57] A possible explanation is that Ni(2)-P bonds are primarily located on the surface of Ni_2P structure,[41] thereby facilitating hydrogen spillover.

The results presented in this study show that Ni_2P crystallite sizes decreased in the following order: Ni_2P/Al_2O_3 > Ni_2P/ZrO_2 > Ni_2P/SiO_2. In other words, the number of Ni(2) sites in these catalysts should be Ni_2P/Al_2O_3 < Ni_2P/ZrO_2 < Ni_2P/SiO_2. This is consistent with the trend of onset temperatures and Ni-adsorbed H species in H_2-TPD profiles, showing that chemisorbed hydrogen atoms desorb easier from Ni_2P/SiO_2 than from Ni_2P/ZrO_2 or Ni_2P/Al_2O_3. This allows Ni_2P/SiO_2 to have better hydrogen transfer ability, promoting DDO and DMO routes for oxygen removal by breaking the $C_{aromatic}$–OH and $C_{aromatic}$–OCH_3 bonds.[25] Because Ni_2P/Al_2O_3 and Ni_2P/ZrO_2 host large Ni_2P particles, less Ni–P–OH species are available for hydrogenation. This allows easy access to Ni sites for chemisorbed guaiacol. The Ni sites in phosphide catalysts cause DME to yield CH_4 and catechol as major products.[47] Cresol formation in guaiacol HDO has not been well explored, possibly because of the various reactions involved and short life times of its precursors.

Time On-Stream Testing. Figure 8 shows the evolution of time on-stream guaiacol conversion and product selectivity over an 8 h period. Selected products included phenol, catechol, benzene, anisole, and cresol, with methane, CO, and saturated compounds excluded for clarity. Within the first hour, X_{GUA} over Ni_2P/SiO_2 was greater than 80%, whereas Ni_2P/Al_2O_3 and Ni_2P/ZrO_2 dropped to 58% and 44%, respectively. After the

dx.doi.org/10.1021/sc300157d | ACS Sustainable Chem. Eng. 2013, 1, 349–358

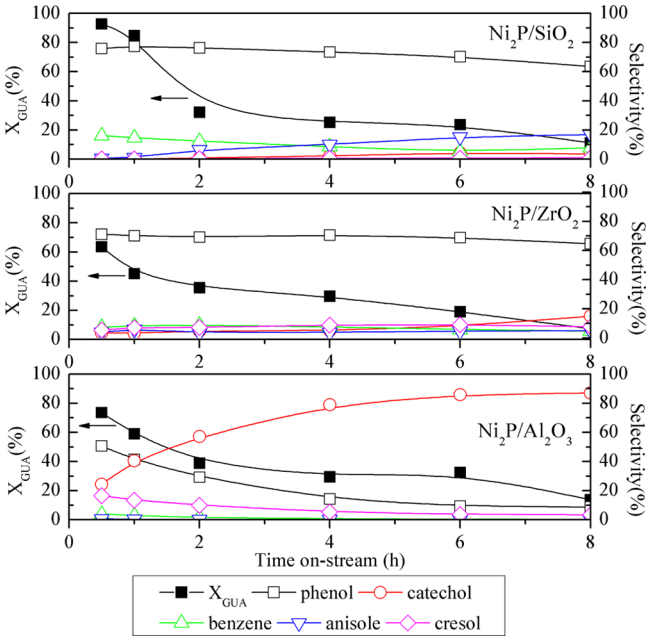

Figure 8. Atmospheric guaiacol HDO over Ni_2P catalysts as a function of time on-stream (reaction temperature: 300 °C; WHSV = 0.67 h^{-1}).

second hour, the conversion for each catalyst gradually decreased to less than 20% at the end of the test.

Phenol and benzene, which accounted for 76% and 16% selectivities, respectively, were the major products initially generated by Ni_2P/SiO_2. Both of these products continuously decreased to 64% and 8%, respectively, and anisole increased to 17% after 8 h testing. Phenol was also a main product over Ni_2P/ZrO_2 and decreased steadily from 71% to 65% over the testing period. Other aromatics were less than 10% at the initial stage; catechol steadily increased from 3% to 15%. Phenol (51%), catechol (24%), and cresol (17%) were the primary products of Ni_2P/Al_2O_3 at the outset. As the reaction time increased, catechol increased to 87%, and phenol and cresol decreased to less than 10%.

Figure S1 of the Supporting Information shows the XRD patterns of freshly prepared and after-testing on-stream Ni_2P catalysts. The index peaks of Ni_2P phase could not be identified for spent catalysts. This may be attributed to severe coke deposition, resulting in the absence of nickel phosphide responses for spent catalysts. Another factor causing deactivation is the change of active phase morphology, possibly because of loss of some P of nickel phosphide to PH_3 under H_2-rich environments.[34,47] Chen et al.[47] compared deactivation behaviors of Ni_2P catalysts and sulfided NiMo catalysts[58] and proposed that phosphide might be oxidized by water, forming less active phosphate or oxy-phosphide compounds.[59] Nevertheless, diffractions of $Ni_{12}P_5$, NiO, and Ni were not apparent, suggesting that coke accumulation is the major factor for catalyst deactivation.

Ni_2P/SiO_2 had higher conversions than Ni_2P/ZrO_2 and Ni_2P/Al_2O_3 within the first hour. Oyama et al.[32] reported that excess P content over Ni_2P/SiO_2 in HDS can replenish the Ni_2P phase to keep it fully phosphided, maintaining its high reactivity. The time on-stream result in this work seems to agree with the aforementioned hypothesis. This provides Ni_2P/SiO_2 with superior reactivity than the other two catalysts at the beginning of on-stream testing.

Phenol and benzene receded and catechol increased with time on-stream for all catalysts. According to the aforementioned hypothesis, loss of phosphide may increase the Ni sites on the surface of Ni_2P catalyst. Therefore, phosphide-derived DDO products (phenol and benzene) were suppressed over time, whereas the metal-catalyzed DME product (catechol) was promoted.

Effects of Supports. Supports are important factors in Ni_2P synthesis. The results of crystallite size, dispersion, and TPR indicate that more acidic support tends to strongly associate with phosphorus, thereby hindering the formation of the Ni_2P phase. Among tested catalysts, Ni_2P/Al_2O_3 required the highest reduction temperature (900 °C) for Ni_2P synthesis; below 900 °C, Ni_2P could not be prepared and only $Ni_{12}P_5$ was observed (results not shown). Relatively weak acidic SiO_2 is an appropriate support. With increasing support acidity, Ni_2P crystallite size increased (i.e., suppressing the interaction between Ni and P).[41] The Ni_2P morphologies varied their chemical natures in atmospheric guaiacol HDO, resulting in varying product distributions. However, no correlation was found between Ni_2P particle size and intrinsic HDO activity. SiO_2 is a promising candidate to provide excess P to keep Ni_2P phosphided for long-term operations.

Coke formation must also be addressed. Increasing acidic strength of supports can promote coke deposition over Ni_2P catalysts. A set of comparison experiments using pure supports as the catalysts in guaiacol HDO was conducted at WHSV = 1.33 h^{-1}. Except SiO_2, which displayed less than 2% X_{GUA}, ZrO_2 and Al_2O_3 showed nearly total conversion of guaiacol. However, more than 95% yields of coke with trace aromatics and methane were identified. Popov et al.[26] reported that guaiacol interacts strongly with the Lewis acid sites on Al_2O_3 (Al^{3+}), yielding doubly anchored phenates at room temperature and subsequently transforming into coke with elevating temperatures. The Lewis acids of ZrO_2 (Zr^{4+}) play the same role as Al^{3+}. In contrast, guaiacol chemisorbs on SiO_2 through H-bonding between silanols (Si−OH) with the methoxyl or hydroxyl group of guaiacol as a form of methoxyphenates. These species do not transform into coke when the temperature is increased.[26] Accordingly, using neutral high surface-area materials (e.g., MCM-41[41] and SBA-15[36]) should be viable for designing Ni_2P catalysts in atmospheric guaiacol HDO.

CONCLUSIONS

This study reports atmospheric guaiacol HDO performed over Ni_2P-supported catalysts. The experiments in this study used three supports, including Al_2O_3, ZrO_2, and SiO_2. Different nickel phosphide morphologies were observed. Ni_2P supported on SiO_2 had the smallest crystallite size, indicating a strong interaction between Ni and P in the active phase. In contrast, the biggest clusters appeared on Al_2O_3, suggesting a weak association between Ni and P. Impurities, such as $AlPO_4$, likely coexisted on Ni_2P/Al_2O_3. Ni_2P on ZrO_2 had its particle size between those on SiO_2 and Al_2O_3. Although Ni_2P supported on these three supports had similar acidity, Ni_2P/SiO_2 had superior H-atom transfer ability.

The catalytic performances of these catalysts showed different outcomes with varying contact times, and this work proposes a network to explain this phenomenon. A detailed analysis based on the pseudo-first-order kinetics of initial conversion and product selectivity suggests that Ni_2P/ZrO_2 is the most reactive, and Ni_2P/SiO_2 is the least reactive. $Ni_2P/$

dx.doi.org/10.1021/sc300157d | ACS Sustainable Chem. Eng. 2013, 1, 349−358

SiO_2 promoted both DMO and DDO routes for oxygen removal, yielding phenol and benzene, respectively, in guaiacol conversion. Ni_2P/ZrO_2 and Ni_2P/Al_2O_3 enhanced the DME route for catechol synthesis. This is possibly related to more square pyramidal Ni(2) (5-P coordinated), which has more P−OH species for hydrogen transfer than quasi-tetrahedral Ni(1) (4-P coordinated) in the small Ni_2P phase of Ni_2P/SiO_2. The time on-stream testing of Ni_2P/SiO_2 also shows superior reactivity than its counterparts within the first hour. In summary, Ni_2P/SiO_2 is the most promising candidate in atmospheric guaiacol HDO.

■ ASSOCIATED CONTENT

Supporting Information

Experimental conditions of activity evaluation and initial selectivity analysis, as well as the XRD patterns of freshly prepared and spent Ni_2P catalysts in the 8 h time on-stream testing. This material is available free of charge via the Internet at http://pubs.acs.org.

■ AUTHOR INFORMATION

Corresponding Author

*E-mail: yclin@saturn.yzu.edu.tw.

Notes

The authors declare no competing financial interest.

■ ACKNOWLEDGMENTS

This work is supported by the Bureau of Energy, Ministry of Economic Affairs (MOEA) and the National Science Council (NSC, Grant 100-2221-E-155-035-MY2) of Taiwan. Valuable suggestions from anonymous reviewers are gratefully appreciated.

■ REFERENCES

(1) Huber, G. W.; Iborra, S.; Corma, A. *Chem. Rev.* **2006**, *106*, 4044−4098.
(2) *Encyclopedia of Energy*; Klass, D. L., Ed.; Elsevier: London, 2004; Vol. *1*.
(3) *Biomass Pyrolysis Liquids Upgrading and Utilisation*; Bridgwater, A. V., Bridge, S. A., Eds.; Elsevier: Amsterdam, 1991.
(4) Bridgwater, A. V. *Appl. Catal., A* **1994**, *116*, 5−47.
(5) Elliott, D. C.; Oasmaa, A. *Energy Fuels* **1991**, *5*, 102−109.
(6) Elliott, D. C.; Beckman, D.; Bridgwater, A. V.; Diebold, J. P.; Gevert, S. B.; Solantausta, Y. *Energy Fuels* **1991**, *5*, 399−410.
(7) Huber, G. W.; Shabaker, J. W.; Dumesic, J. A. *Science* **2003**, *300*, 2075−2077.
(8) Huber, G. W.; Cortright, R. D.; Dumesic, J. A. *Angew. Chem., Int. Ed.* **2004**, *43*, 1549−1551.
(9) Furimsky, E. *Catal. Rev.: Sci. Eng.* **1983**, *25*, 421−458.
(10) Furimsky, E. *Appl. Catal., A* **2000**, *199*, 147−190.
(11) Choudhary, T. V.; Phillips, C. B. *Appl. Catal., A* **2011**, *397*, 1−12.
(12) Hurff, S. J.; Klein, M. T. *Ind. Eng. Chem. Fundam.* **1983**, *22*, 426−430.
(13) Laurent, E.; Delmon, B. *Appl. Catal., A* **1994**, *109*, 77−96.
(14) Elliott, D. C.; Hart, T. R. *Energy Fuels* **2009**, *23*, 631−637.
(15) Vispute, T. P.; Zhang, H. Y.; Sanna, A.; Xiao, R.; Huber, G. W. *Science* **2010**, *330*, 1222−1227.
(16) Elliott, D. C.; Baker, E. G. *Biotechnol. Bioeng. Symp.* **1984**, *14*, 159−174.
(17) Elliott, D. C. *Energy Fuels* **2007**, *21*, 1792−1815.
(18) Zhao, H. Y.; Li, D.; Bui, P.; Oyama, S. T. *Appl. Catal., A* **2011**, *391*, 305−310.
(19) Nimmanwudipong, T.; Runnebaum, R.; Block, D.; Gates, B. *Catal. Lett.* **2011**, *141*, 779−783.
(20) Zhu, X.; Lobban, L. L.; Mallinson, R. G.; Resasco, D. E. *J. Catal.* **2011**, *281*, 21−29.
(21) Gonzalez-Borja, M. A.; Resasco, D. E. *Energy Fuels* **2011**, *25*, 4155−4162.
(22) Nimmanwudipong, T.; Runnebaum, R. C.; Block, D. E.; Gates, B. C. *Energy Fuels* **2011**, *25*, 3417−3427.
(23) Runnebaum, R. C.; Nimmanwudipong, T.; Block, D. E.; Gates, B. C. *Catal. Sci. Technol.* **2012**, *2*, 113−118.
(24) Nimmanwudipong, T.; Aydin, C.; Lu, J.; Runnebaum, R.; Brodwater, K.; Browning, N.; Block, D.; Gates, B. *Catal. Lett.* **2012**, *142*, 1190−1196.
(25) Olcese, R. N.; Bettahar, M.; Petitjean, D.; Malaman, B.; Giovanella, F.; Dufour, A. *Appl. Catal., B* **2012**, *115−116*, 63−73.
(26) Popov, A.; Kondratieva, E.; Goupil, J. M.; Mariey, L.; Bazin, P.; Gilson, J.-P.; Travert, A.; Mauge, F. *J. Phys. Chem. C* **2010**, *114*, 15661−15670.
(27) Popov, A.; Kondratieva, E.; Gilson, J.-P.; Mariey, L.; Travert, A.; Mauge, F. *Catal. Today* **2011**, *172*, 132−135.
(28) Quartararo, J.; Amoureux, J.-P.; Grimblot, J. *J. Mol. Catal., A* **2000**, *162*, 353−365.
(29) Campelo, J. M.; Jaraba, M.; Luna, D.; Luque, R.; Marinas, J. M.; Romero, A. A.; Navio, J. A.; Macias, M. *Chem. Mater.* **2003**, *15*, 3352−3364.
(30) Oyama, S. T. *J. Catal.* **2003**, *216*, 343−352.
(31) Fanchiang, W.-L.; Lin, Y.-C. *Appl. Catal., A* **2012**, *419−420*, 102−110.
(32) Oyama, S. T.; Wang, X.; Lee, Y. K.; Bando, K.; Requejo, F. G. *J. Catal.* **2002**, *210*, 207−217.
(33) Cecilia, J. A.; Infantes-Molina, A.; Rodriguez-Castellon, E.; Jimenez-Lopez, A. *J. Phys. Chem. C* **2009**, *113*, 17032−17044.
(34) Wang, X.; Clark, P.; Oyama, S. T. *J. Catal.* **2002**, *208*, 321−331.
(35) Sawhill, S. J.; Layman, K. A.; Van Wyk, D. R.; Engelhard, M. H.; Wang, C.; Bussell, M. E. *J. Catal.* **2005**, *231*, 300−313.
(36) Koranyi, T. I.; Vit, Z.; Poduval, D. G.; Ryoo, R.; Kim, H. S.; Hensen, E. J. M. *J. Catal.* **2008**, *253*, 119−131.
(37) Villa, R.; Cristiani, C.; Groppi, G.; Lietti, L.; Forzatti, P.; Cornaro, U.; Rossini, S. *J. Mol. Catal., A* **2003**, *204−205*, 637−646.
(38) Lee, Y. K.; Oyama, S. T. *Stud. Surf. Sci. Catal.* **2006**, *159*, 357−360.
(39) Cho, K.-S.; Seo, H.-R.; Lee, Y.-K. *Catal. Commun.* **2011**, *12*, 470−474.
(40) Koranyi, T. I. *Appl. Catal., A* **2003**, *239*, 253−267.
(41) Oyama, S. T.; Lee, Y.-K. *J. Catal.* **2008**, *258*, 393−400.
(42) Kramer, R.; Andre, M. *J. Catal.* **1979**, *58*, 287−295.
(43) Anderson, J. R.; Foger, K.; Breakspere, R. J. *J. Catal.* **1979**, *57*, 458−475.
(44) Miller, J. T.; Meyers, B. L.; Modica, F. S.; Lane, G. S.; Vaarkamp, M.; Koningsberger, D. C. *J. Catal.* **1993**, *143*, 395−408.
(45) Conner, W. C.; Falconer, J. L. *Chem. Rev.* **1995**, *95*, 759−788.
(46) Arai, M.; Fukushima, M.; Nishiyama, Y. *Appl. Surf. Sci.* **1996**, *99*, 145−150.
(47) Li, K.; Wang, R.; Chen, J. *Energy Fuels* **2011**, *25*, 854−863.
(48) Bartholomew, C. H.; Farrauto, R. J. *Fundamentals of Industrial Catalytic Processes*, 2nd ed.; Wiley Interscience: Hoboken, NJ, 2006.
(49) Ward, J. *Zeolite Chemistry and Catalysis*; ACS Monograph: Washington, DC, 1976; Vol. *171*.
(50) Lee, Y.-K.; Oyama, S. T. *J. Catal.* **2006**, *239*, 376−389.
(51) Bui, V. N.; Toussaint, G.; Laurenti, D.; Mirodatos, C.; Geantet, C. *Catal. Today* **2009**, *143*, 172−178.
(52) Bui, V. N.; Laurenti, D.; Afanasiev, P.; Geantet, C. *Appl. Catal., B* **2011**, *101*, 239−245.
(53) Bui, V. N.; Laurenti, D.; Delichere, P.; Geantet, C. *Appl. Catal., B* **2011**, *101*, 246−255.
(54) Lin, Y.-C.; Li, C.-L.; Wan, H.-P.; Lee, H.-T.; Liu, C.-F. *Energy Fuels* **2011**, *25*, 890−896.
(55) Ghampson, I. T.; Sepulveda, C.; Garcia, R.; Radovic, L. R.; Fierro, J. L. G.; DeSisto, W. J.; Escalona, N. *Appl. Catal., A* **2012**, *439*, 111−124.

(56) Ghampson, I. T.; Sepulveda, C.; Garcia, R.; Fierro, J. L.; Escalona, N.; DeSisto, W. J. *Appl. Catal., A* **2012**, *435*, 51−60.
(57) Suzuki, S.; Moula, G. M.; Miyamoto, T.; Nakagawa, Y.; Kinosthita, K.; Asakura, K.; Oyama, S. T.; Otani, S. *J. Nanosci. Nanotechnol.* **2009**, *9*, 195−201.
(58) Laurent, E.; Delmon, B. *J. Catal.* **1994**, *146*, 281−291.
(59) Liu, P.; Rodriguez, J. A.; Takahashi, Y.; Nakamura, K. *J. Catal.* **2009**, *262*, 294−303.